Published online 27 November 2020

Nucleic Acids Research, 2020, Vol. 48, No. 22 ***12957–12971***
doi: 10.1093/nar/gkaa1115

Dual conformational recognition by Z-DNA binding protein is important for the B–Z transition process

Chaehee Park[1], Xu Zheng[2], Chan Yang Park[2], Jeesoo Kim[1], Seul Ki Lee[2], Hyuk Won[2], Jinhyuk Choi[2], Yang-Gyun Kim[2,*] and Hee-Jung Choi[1,*]

[1]Department of Biological Sciences, Seoul National University, Seoul 08826, Korea and [2]Department of Chemistry, Sungkyunkwan University, Suwon 16419, Korea

Received May 20, 2020; Revised October 29, 2020; Editorial Decision October 30, 2020; Accepted November 03, 2020

ABSTRACT

Left-handed Z-DNA is radically different from the most common right-handed B-DNA and can be stabilized by interactions with the Zα domain, which is found in a group of proteins, such as human ADAR1 and viral E3L proteins. It is well-known that most Zα domains bind to Z-DNA in a conformation-specific manner and induce rapid B–Z transition in physiological conditions. Although many structural and biochemical studies have identified the detailed interactions between the Zα domain and Z-DNA, little is known about the molecular basis of the B–Z transition process. In this study, we successfully converted the B–Z transition-defective Zα domain, vvZα$_{E3L}$, into a B–Z converter by improving B-DNA binding ability, suggesting that B-DNA binding is involved in the B–Z transition. In addition, we engineered the canonical B-DNA binding protein GH5 into a Zα-like protein having both Z-DNA binding and B–Z transition activities by introducing Z-DNA interacting residues. Crystal structures of these mutants of vvZα$_{E3L}$ and GH5 complexed with Z-DNA confirmed the significance of conserved Z-DNA binding interactions. Altogether, our results provide molecular insight into how Zα domains obtain unusual conformational specificity and induce the B–Z transition.

GRAPHICAL ABSTRACT

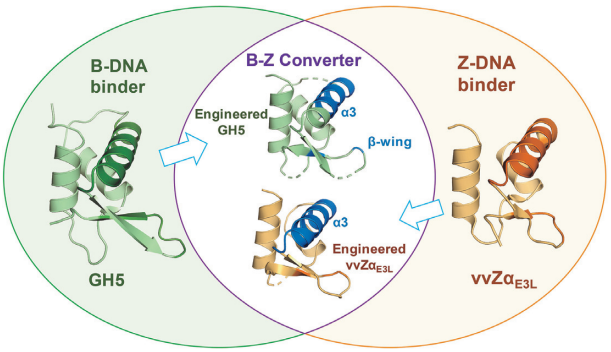

INTRODUCTION

Z-DNA forms biologically active left-handed double helical DNA structures (1–3). Unlike conventional right-handed B-DNA, Z-DNA has alternating *anti*- and *syn*-conformations of nucleotides, forming a unique zig-zag sugar phosphate backbone (4). Although Z-DNA is thermodynamically less stable compared to B-DNA, Z-DNA conformation could be stabilized by interactions with Z-DNA binding proteins under physiological conditions (5–10). Several Z-conformation forming segments (Z-DNA or Z-RNA) have been identified, and their physiological roles are associated with transcriptional regulation and innate immune responses (11,12). In particular, the function of Z-DNA present in a genome has been described as either transcriptional activation or repression, depending on the location and sequence-context of Z-DNA (13). Recently, it has been reported that Z-DNA binding domains (Zα domains) are involved in various cellular functions and diseases including immune responses and cancers by interacting with Z-form nucleic acids (14). For example, recognition of Z-RNA by the Zα domain of ZBP-1 was suggested to be crucial for necroptosis and inflammation (15).

A Zα domain was first identified in human ADAR1 protein (9,10,16,17). Structural studies of the Zα domain of

*To whom correspondence should be addressed. Tel: +82 2 880 6605; Email: choihj@snu.ac.kr
Correspondence may also be addressed to Yang-Gyun Kim. Tel: +82 31 299 4563; Email: ygkimmit@skku.edu

human ADAR1 ($hZ\alpha_{ADAR1}$) revealed that it forms a typical winged helix-turn-helix (wHTH) motif consisting of three α helices (α1, α2 and α3) and a β-wing composed of a loop between two β-strands (β2 and β3) (18,19). Thus, Zα domains belong to the family of the winged helix domain (WHD), which includes functionally diverse nucleic acid binding proteins (20,21). Not surprisingly, the overall fold of the Zα domains closely resembles that of some B-DNA binding WHDs, although there is no detectable sequence homology among them.

In general, Zα domains can both bind to the preformed Z-DNA with a high affinity as a Z-DNA binder and shift the B–Z equilibrium of a potential Z-forming DNA toward Z conformation (referred to as B–Z transition) as a B–Z converter (22,23). However, some Zα domains show different functional characteristics. For example, $hZ\beta_{ADAR1}$, the second Zα domain present in human ADAR1 protein, does not have conformation-specific Z-DNA binding due to the lack of the conserved tyrosine residue located in an α3 helix (24). Another Zα domain, $vvZ\alpha_{E3L}$, present in vaccinia viral E3L protein specifically interacts with the Z-conformation of nucleic acid duplexes, but it completely lacks a B–Z transition activity under physiological conditions (25–29). The NMR structure of the DNA-free form of $vvZ\alpha_{E3L}$ confirmed that it possesses a common fold of the wHTH motif similar to $hZ\alpha_{ADAR1}$ (30). However, the key tyrosine residue of $vvZ\alpha_{E3L}$ was shown to adopt different rotamers, which would reduce Z-DNA binding and result in a lack of B–Z transition activity (26,30). This functional separation of Z-conformation binding activity and B–Z transition activity is unique in $vvZ\alpha_{E3L}$ and raises an interesting question about the molecular mechanism of the B–Z transition.

To date, many structures of several Zα domains complexed with Z-DNA have been determined, greatly improving our understanding of the Z conformation specificity of the Zα domains (18,25,31–38). However, structural information about these detailed interactions is not enough to understand the molecular mechanism of how the B–Z transition proceeds by the Zα domain. A single-molecule study suggested a conformation selection process in which Zα specifically binds to the Z-DNA that is already formed (39). On the other hand, NMR studies and single molecule FRET experiments of $hZ\alpha_{ADAR1}$ suggested an active B–Z transition mechanism, in which $hZ\alpha_{ADAR1}$ first binds to the B-DNA region and then converts it to Z-DNA (40,41). In this context, $hZ\alpha_{ADAR1}$ has been proposed to have a very interesting conformational specificity that binds to both B- and Z-DNA.

In this study, we employed the rational protein engineering strategy to identify what structural factors of the Zα domain are required for B–Z transition activity and which structural features of the Zα domain result in distinguished DNA conformation specificity compared to other nucleic acid binding proteins. First, we separately evaluated Z-DNA binding ability and protein-induced B–Z transition activity using $vvZ\alpha_{E3L}$. Biochemical analyses of engineered $vvZ\alpha_{E3L}$ mutants demonstrate that B-DNA binding ability is important for the B–Z transition activity. Second, using GH5, a canonical B-DNA binding protein with a wHTH motif, as a starting template, we successfully engineered it into a Z-DNA binder and B-to-Z converter by introducing a few point mutations while maintaining the structural integrity of GH5. Functional analyses of GH5 mutants show that key Z-DNA contacting residues on the α3 helix and the β-wing conformation are required for the transformation of a B-DNA binder to a Zα-like protein. To confirm that our engineered $vvZ\alpha_{E3L}$ and GH5 proteins form correctly folded structures and interact with Z-DNA in a manner similar to $hZ\alpha_{ADAR1}$, we determined the crystal structures of the mutants of $vvZ\alpha_{E3L}$ and GH5 complexed with Z-DNA, respectively.

MATERIALS AND METHODS

Protein preparation

The Zα domain of human ADAR1 ($hZ\alpha_{ADAR1}$: amino acids 133–199) was cloned into the pET28a vector. *Escherichia coli* Rosetta (DE3) cells transformed with this construct were grown in LB broth containing 50 μg/ml kanamycin at 37°C until the OD_{600} was around 0.5–0.6 and protein expression was induced by 0.5 mM IPTG. After an additional 4 h incubation at 30°C, cells were harvested and lysed in PBST buffer (1 × phosphate-based saline, 0.05% Tween 20 and 1 mM PMSF) supplemented with DNase I (Roche) using EmulsiFlex-C3 (AVESTIN). Cell lysates were centrifuged at 14,000 rpm for 20 min, and the supernatant was loaded onto Ni-NTA agarose resin (Qiagen) pre-equilibrated with PBST buffer. The resin was washed with 40 mM Imidazole buffer (20 mM Tris–HCl, pH 8.0, 150 mM NaCl, 40 mM Imidazole), and bound protein was eluted from the resin with 250 mM imidazole buffer (pH 8.0). The N-terminal His_6 tag was cleaved by thrombin (Sigma-Aldrich) treatment at 4°C for 16 h in cleavage buffer (20 mM Tris–HCl, pH 8.0, 100 mM NaCl, 2.5 mM $CaCl_2$, 1 mM EDTA), and cleaved protein was further purified with a HiTrap SP column (GE Healthcare) and HiLoad 16/600 Superdex 200 column (GE Healthcare) pre-equilibrated with 20 mM HEPES, pH 7.5 and 150 mM NaCl. Purified protein was dialyzed against DNA binding (DB) buffer (5 mM HEPES, pH 7.5, 20 mM NaCl) at 4°C for 16 h before storage at –80°C.

Purification of $vvZ\alpha_{E3L}$ (aa 2–78 of *Vaccinia virus* protein E3L) and its mutants (Supplementary Table S1) followed the same procedure described above except for the use of a HiTrap Q column (GE Healthcare) instead of a HiTrap SP column.

GH5 (aa 25–100 of the globular domain of *Gallus gallus* histone H5), GH5* and its mutants (Supplementary Table S1) were purified by the same method as described above except for using 20 mM HEPES, pH 8.0 and 150 mM NaCl as gel filtration buffer. The final dialysis into DB buffer was not performed due to protein aggregation at low salt condition.

Circular dichroism measurements

B–Z transition of DNA duplex was monitored based on the CD spectrum using a J-810 CD spectrometer (Jasco). The oligonucleotide of $d(CG)_6$ purchased from IDT was dissolved in CD1 buffer (5 mM HEPES, pH 7.5, 0.1 mM EDTA and 10 mM NaCl) and annealed prior to use. The CD measurements of DNA duplex in the presence of

vvZα$_{E3L}$ and its mutant proteins were carried out at 25°C. Specifically, 20 μM of the DNA duplex substrate in a CD1 buffer was used for the CD measurement with a 0.1-cm quartz cell. To prevent a substantial change in buffer composition due to the addition of protein sample, the maximum volume of protein did not exceed 5% of the total volume. Before each measurement, samples were incubated for 1 h at 25°C. CD spectra between 230 and 320 nm were recorded three times and averaged. The CD measurements of GH5* and its mutant proteins were carried out in different conditions to prevent aggregation of protein/DNA complex. CD spectra were collected using a 1-cm quartz cell, and 1 μM of the DNA duplex substrate was dissolved in CD2 buffer (5 mM HEPES, pH 8.0, 50 mM NaCl and 0.1 mM EDTA). All other details for CD measurements are the same as in the CD experiment of vvZα$_{E3L}$. The relative transition activity of each protein was calculated by comparison of each CD signal at 255 nm with that of hZα$_{ADAR1}$ (set to 100%) during the B–Z transition. When analyzing changes in the CD signals at 255 nm, the CD signals by the protein samples were ignored because they were negligibly small (Supplementary Figure S1) (22). The relative amount of proteins to nucleic acids used for CD measurement was indicated as [P]/[N] ratio, which is the molar ratio of protein monomer to double-stranded DNA of *d*(CG)$_6$. This definition was used throughout this study.

Double-stranded DNA preparation

DNA oligonucleotides for crystallization, *d*(TCGCGCG); for CD measurements, *d*(CG)$_6$; and for MST measurements, 5′-Alexa647-labeled *d*(TATGCAATCGTAATAA ACCGT), and its non-labeled complementary DNA were purchased from IDT. 5′-Cy5-labeled *d*[T(Br^{5}CG)$_{15}$] was purchased from Gene Link. DNA samples were dissolved in DB buffer (for crystallization and MST) or CD1 buffer (for CD). Dissolved DNAs were fully denatured at 95°C for 5 min and were annealed by gradual cooling to 4°C to make double-stranded DNA. DNA duplex samples at appropriate concentrations (1.2 mM for crystallization, 50 μM for MST and 1 mM for CD) were stored at –20°C or used immediately.

Crystallization

Purified vvZα$_{E3L}$:α3$_{ADAR1}$ (0.6 mM) was mixed with [*d*(TCGCGCG)]$_2$ at a 2:1 molar ratio and incubated at room temperature for 1 h before crystallization. Crystals were obtained by the hanging drop vapor diffusion method at 22°C using 0.1 M sodium citrate (pH 4.0), 0.8 M ammonium sulfate and 10% ethylene glycol as a reservoir solution.

Similarly, purified GH5*:α3N$_{ADAR1}$-PW (0.3 mM) was mixed with [*d*(TCGCGCG)]$_2$ at a 2:1 molar ratio and incubated at room temperature for 1 h before crystallization. Crystals were obtained by the hanging drop vapor diffusion method at 22°C using 0.1 M MES (pH 6.0), 20% PEG 4000 and 5% ethylene glycol as a reservoir solution.

Data collection and structure determination

Crystals of vvZα$_{E3L}$:α3$_{ADAR1}$/[*d*(TCGCGCG)]$_2$ complex and GH5*:α3N$_{ADAR1}$-PW/[*d*(TCGCGCG)]$_2$ complex were frozen using 20–25% ethylene glycol as a cryoprotectant. Diffraction data sets were collected on beamline 5C at the Pohang Accelerator Laboratory (PAL, Korea). Images were processed using HKL2000 (42) and the CCP4 suite (43). The complex structures of vvZα$_{E3L}$:α3$_{ADAR1}$/[*d*(TCGCGCG)]$_2$ and GH5*:α3N$_{ADAR1}$-PW/[*d*(TCGCGCG)]$_2$ were solved by molecular replacement with the PHENIX program (44) using the structure of the Zα domain of ADAR1 (PDB ID 1QBJ) and globular domain of histone H5 (PDB ID 1HST) as a search model, respectively. Several cycles of manual model rebuilding with COOT (45) and refinement with PHENIX (44) were performed, and each final model was validated by MolProbity (46). The final model of the vvZα$_{E3L}$:α3$_{ADAR1}$/[*d*(TCGCGCG)]$_2$ complex consisting of three copies of vvZα$_{E3L}$:α3$_{ADAR1}$ and three copies of *d*(TCGCGCG) was deposited in the PDB with PDB ID 7C0I, and the model of GH5*:α3N$_{ADAR1}$-PW/[*d*(TCGCGCG)]$_2$ complex containing 2 copies of GH5*:α3N$_{ADAR1}$-PW and 1 copy of [*d*(TCGCGCG)]$_2$ was deposited in the PDB with PDB ID 7C0J. Data collection and refinement statistics are shown in Supplementary Tables S2 and S3.

Affinity measurement by MicroScale Thermophoresis (MST)

Affinity measurements by MST (47) were performed using a Monolith NT.115 pico instrument (NanoTemper). Each labeled dsDNA sample, *d*(5′-Alexa647-TATGCAATCGT AATAAACCGT)::*d*(ACGGTTTATTACGATTGCATA) (named B-DNA) (39) and [*d*(5′-Cy5-(Br^{5}CG)$_{15}$]$_2$ (named Z-DNA), was used at a concentration of 5 nM. *d*(CG) repeat DNA duplexes containing Br^{5}C bases are known to form stable Z-conformations in physiological conditions (48). The prepared protein was titrated in 1:1 serial dilution in DB buffer. In the case of GH5*:α3N$_{ADAR1}$-PW, the DB buffer was substituted by a high-salt buffer consisting of 20 mM HEPES (pH 8.0) and 100 mM NaCl or a high-salt KCl buffer consisting of 20 mM Tris–HCl (pH 7.8) and 150 mM KCl. All buffers used in the experiments were supplemented with 0.5 mg/ml BSA and 0.05% (v/v) Tween 20. After 15 min (vvZα$_{E3L}$ and its mutants) or 10 min (GH5* and its mutants) incubation at room temperature in the dark, each protein/DNA mixture was added into a Monolith NT.115 standard capillary. The measurements were performed at 5% LED power and 40% MST power (vvZα$_{E3L}$:α3$_{ADAR1}$) or 80% MST power (GH5*:α3N$_{ADAR1}$-PW) at 22°C. Data analysis by nonlinear regression was performed using MO.Affinity Analysis provided by NanoTemper and GraphPad Prism (GraphPad Software, USA).

Multi-angle light scattering coupled with size exclusion chromatography (SEC-MALS)

MALS experiments were performed with miniDAWN TREOS (Wyatt Technology, Co.) to determine the absolute molecular mass. Each protein sample was loaded into a Superdex 200 Increase 10/300 GL column (GE healthcare) pre-equilibrated with 20 mM HEPES (pH 7.5) and 100 mM NaCl. The light scattering signal and UV absorbance at 280

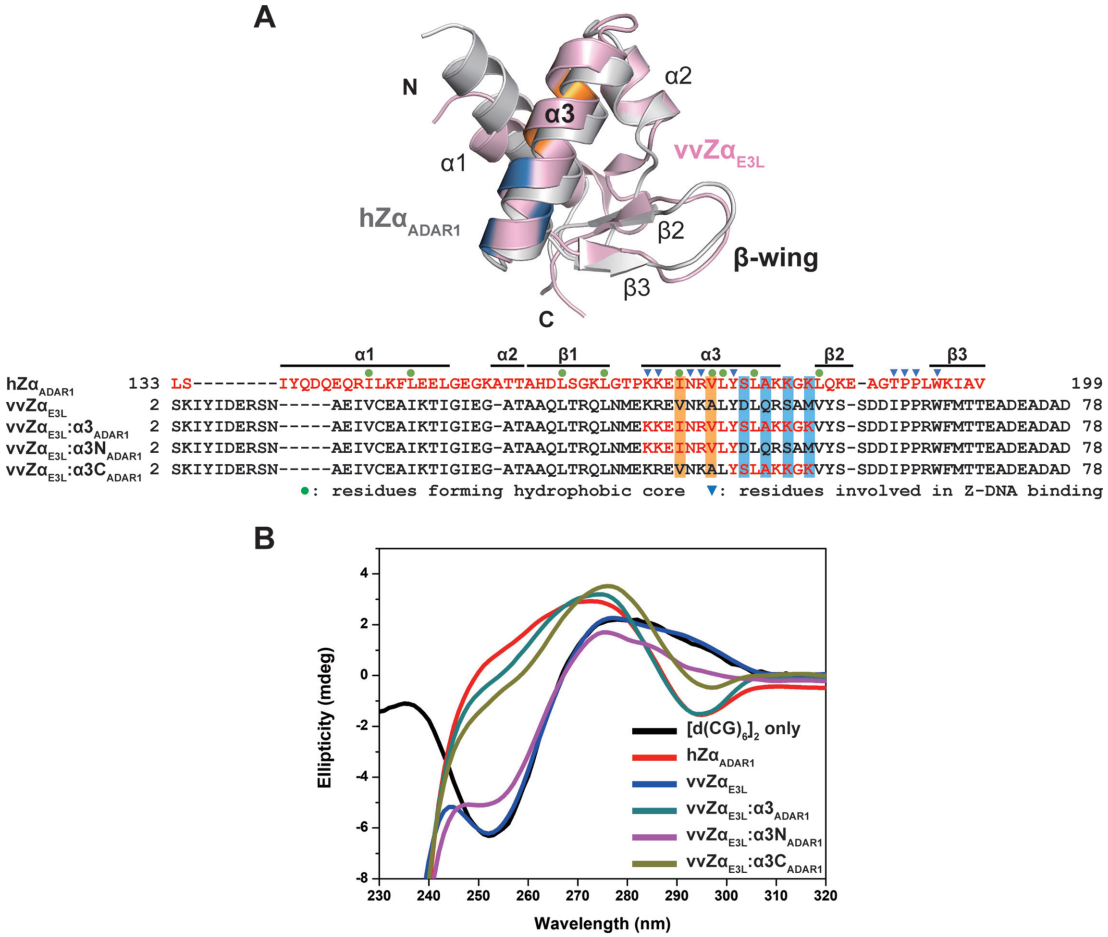

Figure 1. Design of α3-swapped vvZα$_{E3L}$ mutants and their CD spectra. (**A**) Structural and sequence comparison of hZα$_{ADAR1}$ and wild-type and chimeric mutants of vvZα$_{E3L}$. Structural alignment of free vvZα$_{E3L}$ (PDB ID 1OYI, light pink) and hZα$_{ADAR1}$ (PDB ID 1QBJ, gray) and sequence alignment of hZα$_{ADAR1}$, vvZα$_{E3L}$ and α3-swapped vvZα$_{E3L}$ mutants (vvZα$_{E3L}$:α3$_{ADAR1}$, vvZα$_{E3L}$:α3N$_{ADAR1}$, and vvZα$_{E3L}$:α3C$_{ADAR1}$) are shown. In chimeric mutants, amino acids derived from hZα$_{ADAR1}$ are in red. Residues involved in hydrophobic core formation in hZα$_{ADAR1}$, but are not conserved in vvZα$_{E3L}$ are highlighted in orange. The residues highlighted in blue are the C-terminal residues of the α3 helix that are not conserved between hZα$_{ADAR1}$ and vvZα$_{E3L}$. These residues are represented in the ribbon diagram with the same color code. (**B**) CD spectra of *d*(CG)$_6$ in the presence of α3-swapped vvZα$_{E3L}$ mutants. The transition of *d*(CG)$_6$ from B-conformation to Z-conformation was monitored in the presence of various proteins at a [P]/[N] ratio of 4 using CD. The B–Z transition of *d*(CG)$_6$ induced by vvZα$_{E3L}$ mutants are compared with that by hZα$_{ADAR1}$.

nm were measured, and data were analyzed using Astra 6 software (Wyatt Technology, Co.) to assess molar mass.

RESULTS

B–Z transition activity of α3 helix-swapped mutants of vvZα$_{E3L}$

We first confirmed that vvZα$_{E3L}$ lacks B–Z transition activity under physiological conditions even with an excess molar ratio of [P]/[N] (Supplementary Figure S1). To investigate structural elements responsible for B–Z transition activity that are present in hZα$_{ADAR1}$ and absent in vvZα$_{E3L}$, we designed several chimeric mutants of vvZα$_{E3L}$ and hZα$_{ADAR1}$ and monitored their B–Z transition activities by CD spectroscopy. Based on structural information of hZα$_{ADAR1}$ in complex with Z-DNA, we reasonably assumed that the regions of the α3 helix would be crucial for the B–Z transition (18,25,31–38). Thus, we initially created an α3-helix-swapped mutant of vvZα$_{E3L}$ (vvZα$_{E3L}$:α3$_{ADAR1}$), in which the α3 helix of vvZα$_{E3L}$ was replaced by the corresponding helix of hZα$_{ADAR1}$ (Figure 1A, Supplementary Table S1, and Supplementary Figure S2). Whereas the wild-type vvZα$_{E3L}$ has no detectable B–Z transition activity, the B–Z transition activity of vvZα$_{E3L}$:α3$_{ADAR1}$ was observed by CD spectroscopy using [*d*(CG)$_6$]$_2$ at a molar ratio of [P]/[N] = 4, i.e. four protein molecules for one double-stranded DNA molecule, which was previously reported as the stoichiometry between the Zα domain and Z-DNA (18,22,35). The B–Z transition activity of this chimera was similar to that of hZα$_{ADAR1}$ when CD signals at 255 nm were compared (Figure 1B and Table 1). The CD titration profile of this mutant indicated that the B–Z transition reached saturation at a [P]/[N] ratio of 4 (Supplementary Figure S1). To further study the role of the α3 helix, two chimeric mutants containing either the C-terminal part (vvZα$_{E3L}$:α3C$_{ADAR1}$) or the N-terminal part (vvZα$_{E3L}$:α3N$_{ADAR1}$) of the α3 helix of hZα$_{ADAR1}$ were constructed (Figure 1A), and we examined their B–Z transition activities. The CD spectrum by vvZα$_{E3L}$:α3C$_{ADAR1}$

Table 1. Relative B–Z transition activity of each vvZα$_{E3L}$ mutant compared to that of hZα$_{ADAR1}$

Protein	B–Z conversion (%)
hZα$_{ADAR1}$	100±4.0[a]
vvZα$_{E3L}$	0±0.1
vvZα$_{E3L}$:α3$_{ADAR1}$	78±3.1
vvZα$_{E3L}$:α3N$_{ADAR1}$	17±0.8 (61±2.3[b])
vvZα$_{E3L}$:α3C$_{ADAR1}$	71±2.8
vvZα$_{E3L}$-D49S	46±1.9 (70±2.7[b])
vvZα$_{E3L}$-D49R	35±1.5 (71±2.8[b])
vvZα$_{E3L}$-S53K	16±0.8 (65±2.5[b])
vvZα$_{E3L}$-M55K	7±0.3 (57±2.2[b])
vvZα$_{E3L}$-S53K/M55K	33±1.4 (72±2.9[b])
vvZα$_{E3L}$-S49S/S53K/M55K	67±2.6
vvZα$_{E3L}$-D49R/S53K/M55K	71±2.9
vvZα$_{E3L}$-V43I	2±0.2 (53±2.1[b])
vvZα$_{E3L}$-V43I/A46V	4±0.3 (57±2.3[b])
vvZα$_{E3L}$-A46V/53K	39±1.6 (71±2.8[b])
vvZα$_{E3L}$-A46V/S53K/M55K	69±2.7

[a]The relative B–Z transition activity compared to that of hZα$_{ADAR1}$ at a [P]/[N] ratio of 4.
[b]The number in parentheses indicates the B–Z transition activity at a [P]/[N] ratio of 30.

showed a high degree of B–Z transition, almost identical to that of vvZα$_{E3L}$:α3$_{ADAR1}$ (Figure 1B). On the other hand, vvZα$_{E3L}$:α3N$_{ADAR1}$ induced a relatively small conformational change from B-DNA to Z-DNA (Figure 1B), classifying this chimera as a weak B–Z converter. Moreover, vvZα$_{E3L}$:α3N$_{ADAR1}$ requires excess [P]/[N] ratio to reach saturation in CD titration experiment. (Supplementary Figure S1). Altogether, we concluded that the C-terminal part of the α3 helix of hZα$_{ADAR1}$ (α3C$_{ADAR1}$) is more important for B–Z transition activity than is the α3N$_{ADAR1}$.

Effect of charge distribution in the C-terminal part of the α3 helix on B–Z transition activity

To identify which amino acids in α3 helix-swapped mutants of vvZα$_{E3L}$ are critical for B–Z transition activity, we generated point mutations in the α3 helix of vvZα$_{E3L}$. Although the last C-terminal turn of the α3 helix (S178–K182 in hZα$_{ADAR1}$) had no direct contact with Z-DNA based on the published structures of Zα/Z-DNA complexes, we postulated that positively charged residues of the α3C$_{ADAR1}$ may play an important role in B–Z transition based on the CD results of vvZα$_{E3L}$:α3C$_{ADAR1}$. To test our hypothesis, several vvZα$_{E3L}$ mutants containing individual or combined point mutations of D49S, D49R, S53K and M55K, which correspond to S178, K182 and K184 of hZα$_{ADAR1}$, respectively, were generated (Supplementary Table S1 and Supplementary Figure S2). These vvZα$_{E3L}$ mutants with a single point mutation (vvZα$_{E3L}$-D49S, -D49R, -S53K, and -M55K) generally exhibited weak B–Z transition activities at a 4 [P]/[N] molar ratio as assessed by CD (Figure 2A and Table 1). In contrast, a double-point mutant, vvZα$_{E3L}$-S53K/M55K, showed enhanced B–Z transition activity (Figure 2B and Table 1). Finally, the triple-point mutants (vvZα$_{E3L}$-D49R/S53K/M55K and vvZα$_{E3L}$-D49S/S53K/M55K) were able to convert B-DNA to Z-DNA at a 4 [P]/[N] molar ratio in a manner similar to those of vvZα$_{E3L}$:α3$_{ADAR1}$ and vvZα$_{E3L}$:α3C$_{ADAR1}$ (Figure 2B). These results indicate that removal of negatively charged residue and the addition of positively charged residues (D49R, S53K and M55K) in the α3C region of vvZα$_{E3L}$ greatly enhance B–Z transition activity.

Effect of hydrophobic residues in the N-terminal part of the α3 helix on B–Z transition activity

The structure of hZα$_{ADAR1}$ revealed that nonpolar residues in α1 (I143 and L147), α2 (L161 and L165) and α3 (I172, V175, L176, and L179) helices and L185 of the β2 strand formed a hydrophobic core, which may be important for maintaining structural integrity (19). The sequence comparison of vvZα$_{E3L}$ with hZα$_{ADAR1}$ showed that hydrophobic core-forming Leu residues of hZα$_{ADAR1}$ are mostly conserved in vvZα$_{E3L}$ (L32, L36, L47 and L50), but two amino acids in the α3N region of vvZα$_{E3L}$ has smaller aliphatic residues (V43 and A46) than hZα$_{ADAR1}$ (I172 and V175) (Figure 1). To examine the importance of the hydrophobic residues in the α3N for B–Z transition activity, vvZα$_{E3L}$ mutants with different hydrophobicity at α3N were created (V43I and A46V) (Supplementary Table S1 and Supplementary Figure S2). Single (vvZα$_{E3L}$-V43I) or double point mutation (vvZα$_{E3L}$-V43I/A46V) did not improve the B–Z transition activity at a 4 [P]/[N] molar ratio (Figure 2C). However, at a 30 [P]/[N] molar ratio, vvZα$_{E3L}$-V43I and vvZα$_{E3L}$-V43I/A46V showed substantial B–Z transition activities, although the transition was not complete (Figure 2C). These results suggested that a more stable hydrophobic core formed by the bigger hydrophobic residues in the α3N contributes to the B–Z transition process.

Next, we generated combination mutants of vvZα$_{E3L}$ having hydrophobic residues in the α3N and positively charged residues in the α3C. Two mutants, vvZα$_{E3L}$-A46V/S53K and vvZα$_{E3L}$-A46V/S53K/M55K, showed drastically enhanced B–Z transition compared with single point mutants at a 4 [P]/[N] molar ratio (Figure 2D and Table 1). This result suggests that the N-terminal hydrophobic residues and the C-terminal positively charged residues of the α3 helix improved the B–Z transition activity in a synergistic manner. Thus, we identified key amino acid residues of the Zα domain that affect the B–Z transition.

B-DNA binding affinity of the α3 helix-swapped vvZα$_{E3L}$ mutants

In the previous sections, we showed that the introduction of positive charges into the α3C region of vvZα$_{E3L}$ enhanced B–Z transition activity. To test whether increased B–Z transition activity is related to the DNA binding affinity, we determined the DNA binding affinity of each α3 chimeric vvZα$_{E3L}$ mutant (vvZα$_{E3L}$:α3$_{ADAR1}$, vvZα$_{E3L}$:α3N$_{ADAR1}$ and vvZα$_{E3L}$:α3C$_{ADAR1}$) using MST (47). As summarized in Table 2, vvZα$_{E3L}$:α3$_{ADAR1}$ and vvZα$_{E3L}$:α3C$_{ADAR1}$ have significantly enhanced B-DNA binding affinities, with K_D values of 2.6 μM and 1.1 μM, respectively. Interestingly, these K_D values are almost the same as that of hZα$_{ADAR1}$ for the interaction with B-DNA (K_D of 1.8 μM). In contrast, the wild-type vvZα$_{E3L}$ had a much lower affinity to B-DNA (K_D of 20 μM) (Table 2 and Supplementary Figure S3). The chimeric mutant,

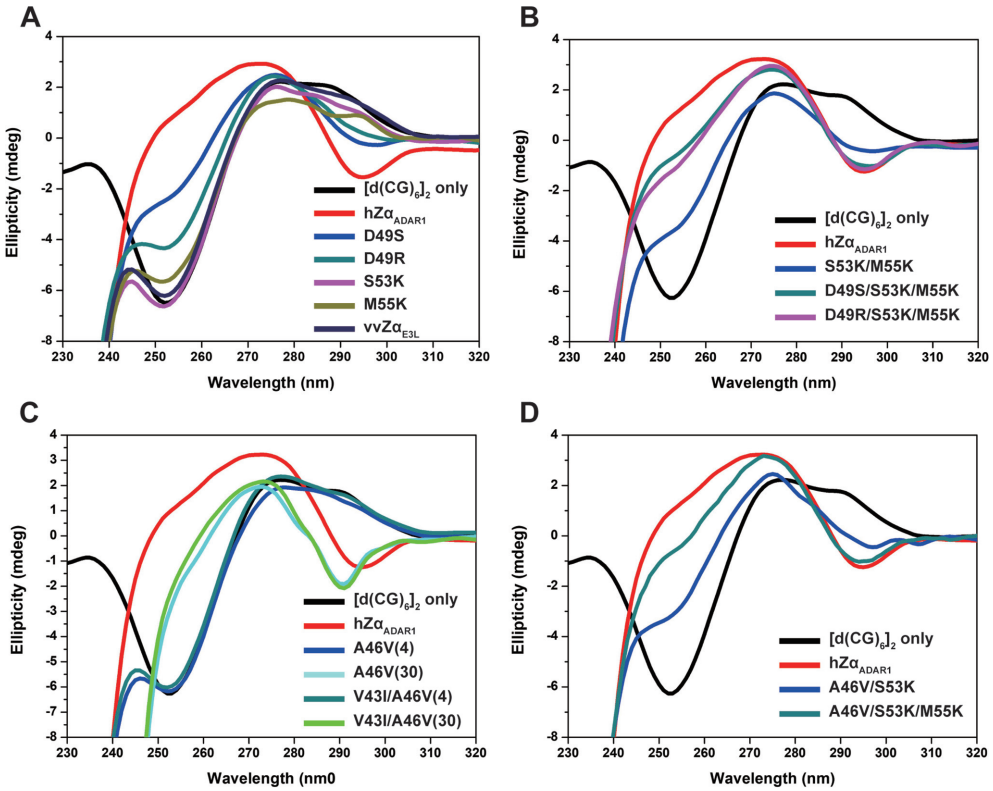

Figure 2. CD analysis for the B–Z transition of $[d(CG)_6]_2$ by $vvZ\alpha_{E3L}$ mutants. CD spectra of $d(CG)_6$ measured in the presence of (**A**) single-point mutation and (**B**) double- and triple-point mutations of $vvZ\alpha_{E3L}$, which have reduced negative charge or increased positive charges are presented. Changes in the CD signals at 255 and 292 nm represent the B–Z transition of $[d(CG)_6]_2$. CD spectra of $[d(CG)_6]_2$ alone (B-DNA, Supplementary Figure S1) and in the presence of $hZ\alpha_{ADAR1}$ or $vvZ\alpha_{E3L}$ at a [P]/[N] ratio of 4 are shown as controls. (**C**) CD spectra of $d(CG)_6$ measured in the presence of the hydrophobic core mutants of $vvZ\alpha_{E3L}$ at [P]/[N] ratios of 4 and 30 are shown. The numbers 4 and 30 in parentheses represent the [P]/[N] ratios. (**D**) CD spectra of $d(CG)_6$ measured in the presence of the combination-mutants of $vvZ\alpha_{E3L}$ containing both positively charged and hydrophobic core mutations at a [P]/[N] ratio of 4 are shown.

$vvZ\alpha_{E3L}$:$\alpha 3N_{ADAR1}$, which did not exhibit an observable B–Z transition activity at a 4 [P]/[N] molar ratio, showed little improvement in B-DNA binding affinity with a K_D of 17 μM. Therefore, the results of our affinity measurements in combination with CD data suggest that improved B-DNA binding affinities of $vvZ\alpha_{E3L}$ mutants ($vvZ\alpha_{E3L}$:$\alpha 3_{ADAR1}$ and $vvZ\alpha_{E3L}$:$\alpha 3C_{ADAR1}$) are closely related to the increment of B–Z transition activity. Although these two mutants showed improvement in Z-DNA binding by 2–3 times compared to $vvZ\alpha_{E3L}$, they still have 10-fold lower affinities for Z-DNA than $hZ\alpha_{ADAR1}$ (Table 2). Thus, high affinity binding to Z-DNA may not be necessary for B–Z transition activity. Based on our observations, we postulated that positively charged residues in the $vvZ\alpha_{E3L}$:$\alpha 3_{ADAR1}$ mutant may be involved in increased B-DNA binding affinity and thus may promote the B–Z transition process.

Table 2. DNA binding affinities of $hZ\alpha_{ADAR1}$ and wild-type and chimeric mutants of $vvZ\alpha_{E3L}$

Protein	Z-DNA binding affinity (μM)	B-DNA binding affinity (μM)
$hZ\alpha_{ADAR1}$	0.018 ± 0.001	2.7 ± 0.5
$vvZ\alpha_{E3L}$	2.0 ± 0.1	21 ± 0.5
$vvZ\alpha_{E3L}$:$\alpha 3_{ADAR1}$	1.0 ± 0.05	2.4 ± 0.2
$vvZ\alpha_{E3L}$:$\alpha 3N_{ADAR1}$	0.94 ± 0.01	18 ± 1.0
$vvZ\alpha_{E3L}$:$\alpha 3C_{ADAR1}$	0.74 ± 0.01	1.3 ± 0.2

All experiments were performed at 22°C with buffer consisting of 5 mM HEPES (pH 7.5), 20 mM NaCl, 0.5 mg/ml BSA and 0.05% Tween20.

Crystal structure of engineered vvE3L in complex with $[d(TCGCGCG)]_2$

To understand the functional acquisition of B–Z transition activity of chimeric $vvZ\alpha_{E3L}$ at the molecular level, we determined the crystal structure of $vvZ\alpha_{E3L}$:$\alpha 3_{ADAR1}$ in complex with $[d(TCGCGCG)]_2$ at 2.4 Å resolution (Supplementary Table S2). Unexpectedly, a monomeric form of $vvZ\alpha_{E3L}$ chimera (chain A) and a domain-swapped dimer (chains B and C) were present with three left-handed $d(TCGCGCG)$ molecules in an asymmetric unit of the crystal lattice (Figure 3A). In solution, $vvZ\alpha_{E3L}$:$\alpha 3_{ADAR1}$ showed increased absolute molar mass in a concentration dependent manner as analyzed by SEC-MALS, suggesting that $vvZ\alpha_{E3L}$:$\alpha 3_{ADAR1}$ is likely to dimerize at high concentrations (Supplementary Figure S4). A composite model consisting of the N-terminal part of chain B (3–36) and the C-terminal part of chain C (37–70) or vice versa was well aligned to the monomeric form of chimera (chain A) with an RMSD of 0.47 Å (Supplementary Figure S5).

By analyzing three molecules of the chimera/Z-DNA complex in an asymmetric unit, we discovered that the Z-

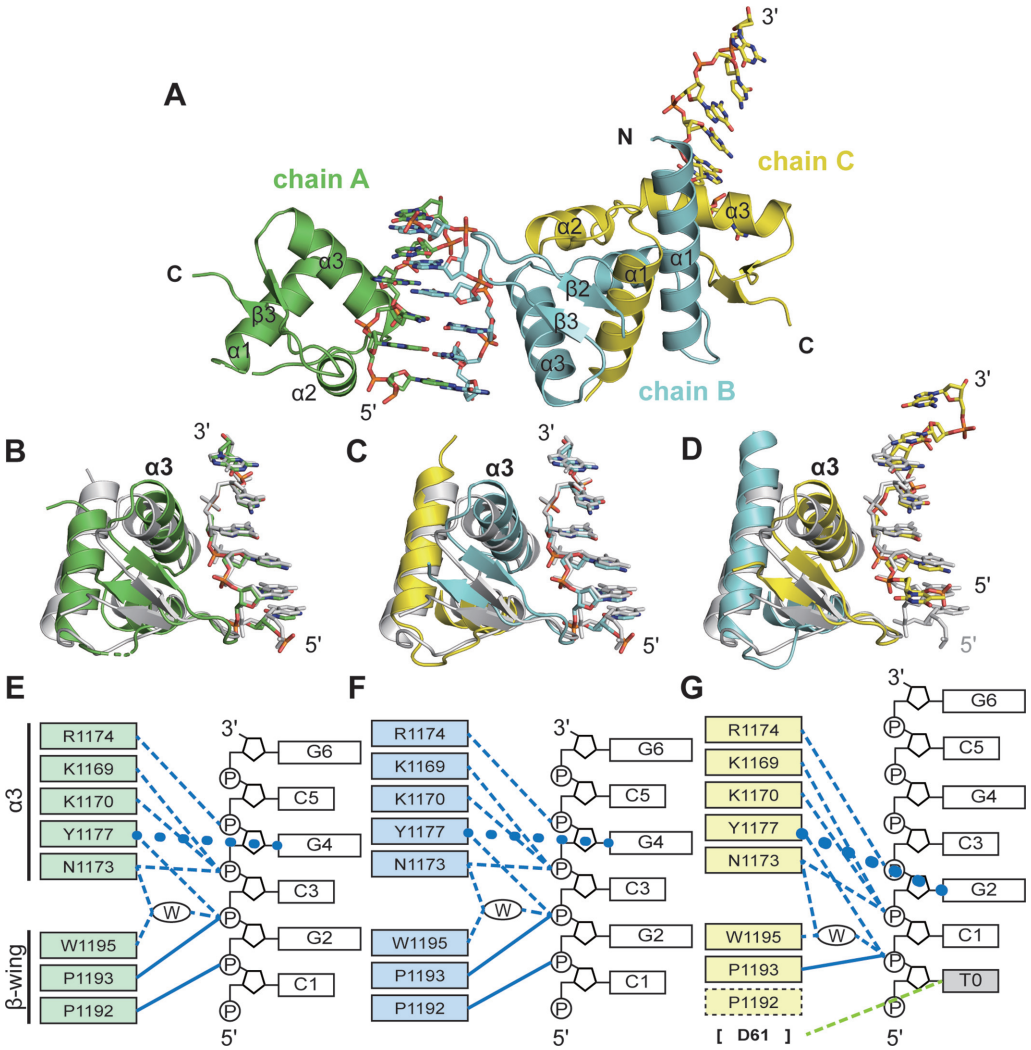

Figure 3. Crystal structure of vvZα$_{E3L}$ mutant in complex with Z-DNA (vvZα$_{E3L}$:α3$_{ADAR1}$/Z-DNA). (**A**) Overall structure of vvZα$_{E3L}$:α3$_{ADAR1}$ complexed with [*d*(TCGCGCG)]$_2$. Monomeric (chain A in green) and domain-swapped dimeric (chains B and C in cyan and yellow, respectively) vvZα$_{E3L}$ mutant and Z-DNA of *d*(TCGCGCG) (chains D, E, and F) in an asymmetric unit of the crystal lattice are shown. (**B–D**) The complex structure of each DNA chain and its binding partner protein (chain A or composite models) is aligned to the complex structure of hZα$_{ADAR1}$ and *d*(TCGCGCG) (PDB ID 1QBJ). One composite model consists of chain B (aa 37–69) and chain C (aa 6–36), and the other consists of chain B (aa 3–36) and chain C (aa 37–70). (**E–G**) Protein–DNA interactions are shown as schematic diagrams. Hydrogen bonds are shown as dashed lines, van der Waals contacts are shown as solid lines, and the CH–π interactions are shown as circled lines. Water molecule within the protein–DNA interface is marked with a W inside the oval. In the chimeric mutant of vvZα$_{E3L}$, amino acids derived from hZα$_{ADAR1}$ are indicated by adding 1,000 to the amino acid numbers of hZα$_{ADAR1}$ to clarify that those residues are from foreign protein. Residues involved in Z-DNA binding are indicated by colored boxes and the residue, which does not participate in the interaction with Z-DNA is shown by dotted box. Non-canonical interaction of D61 (shown in brackets), which is not conserved between hZα$_{ADAR1}$ and vvZα$_{E3L}$ is indicated by a green dashed line.

DNA binding interface in one of three complex molecules (Chains C and F) was shifted by two bases, interacting with T0 as well as P1 and P2 (Figure 3D and G). Specifically, Y1177 of vvZα$_{E3L}$ chimera (corresponding to Y48 of vvZα$_{E3L}$) makes close contact with G2 instead of G4, and the N1173 of the vvZα$_{E3L}$ chimera (corresponding to N44 of vvZα$_{E3L}$) interacts with P2 instead of P4. (The residues derived from hZα$_{ADAR1}$ in the vvZα$_{E3L}$ chimera are numbered by adding 1,000 to the original residue numbers of hZα$_{ADAR1}$). Although this unusual complex may be formed by crystallographic packing, it is interesting to note that the binding interface between chains C and F looks similar to that of the complex found in the B–Z junction (Supplementary Figure S6). In the remaining two complexes, a conventional Z-DNA binding interface was formed by K1169, N1173, Y1177, W1195 of the vvZα$_{E3L}$ chimera and P3, P4, and G4 of Z-DNA (Figure 3B, C, E, and F).

Three molecules of *d*(TCGCGCG) in our complex structure are well aligned to each other with RMSD values in the range of 0.3–0.4 Å. When comparing vvZα$_{E3L}$ chimera-bound Z-DNA with hZα$_{ADAR1}$-bound Z-DNA, protein-free Z-DNA (PDB ID 4FS6), and ideal B-DNA generated by the Coot program (45), it was clear that the DNA in complex with vvZα$_{E3L}$:α3$_{ADAR1}$ formed a Z-conformation similar to a Zα-bound or a protein-free Z-DNA structure, with RMSD values of 0.6 Å and 0.8 Å, respectively (Supple-

mentary Table S4). Analysis of the vvZα$_{E3L}$ chimera-bound Z-DNA structure using the web 3DNA 2.0 program (49), which provides various parameters related to DNA structure including 'Rise' and 'Twist,' showed that the 'Rise' values are between those in the protein-free state and in the hZα$_{ADAR1}$-bound state (Supplementary Figure S7).

When a monomeric form of vvZα$_{E3L}$:α3$_{ADAR1}$ (chain A) was aligned to hZα$_{ADAR1}$ in a complex with *d*(TCGCGCG), the RMSD value was calculated as 0.52 Å. In contrast, an RMSD value of 1.87 Å was obtained by aligning vvZα$_{E3L}$:α3$_{ADAR1}$ with vvZα$_{E3L}$ in the DNA-free state. This comparison clearly shows that vvZα$_{E3L}$:α3$_{ADAR1}$ is structurally more similar to hZα$_{ADAR1}$; the sequence identity between vvZα$_{E3L}$:α3$_{ADAR1}$ and hZα$_{ADAR1}$ is only 43% compared with 75% between vvZα$_{E3L}$:α3$_{ADAR1}$ and vvZα$_{E3L}$ (Figure 1A). The large structural deviation between vvZα$_{E3L}$:α3$_{ADAR1}$ and DNA-free vvZα$_{E3L}$ comes from the difference in relative position between α1 and α3 helices and the positional shift of the β-wing. When α3 helices were aligned together, the α1 helix was located much closer to the α3 helix in the vvZα$_{E3L}$ chimera, forming a tightly packed hydrophobic core (Supplementary Figure S8). V43I and A46V mutations of the α3 helix in vvZα$_{E3L}$ chimera contributed to the formation of the extensive hydrophobic interaction network, re-locating the α2 helix and bringing the α1 helix closer to the α3 helix. As a result, A12, V15 and M38, which do not make contact with V47 and A50 in the vvZα$_{E3L}$ structure, interact with the corresponding residues, I1172 and V1175, of the vvZα$_{E3L}$ chimera (Supplementary Figure S9).

Altogether, our structure shows that the engineered vvZα$_{E3L}$ chimera, vvZα$_{E3L}$:α3$_{ADAR1}$, forms a Zα-like structure, which may be related to the functional acquisition of B–Z conversion activity of this chimera.

Construction of a chimeric protein of GH5 that enables B–Z transition

It is noteworthy that some B-DNA binding proteins containing a wHTH motif show high structural similarity to hZα$_{ADAR1}$ (18,20). In the previous sections, chimeric mutants of vvZα$_{E3L}$ having the enhanced B-DNA binding affinity showed B–Z transition activity. Thus, we hypothesized that it would be possible to engineer B-DNA binding proteins with high structural homology to Zα domain into Zα-like proteins with B–Z transition activity by adding Z-DNA binding ability. To demonstrate our hypothesis, we created a new Zα-like protein by introducing a number of mutations into the B-DNA binding protein with a wHTH motif.

We chose GH5, the globular domain of the linker histone H5, as a target B-DNA binder to engineer into a Z-DNA binding protein because a structural analysis of GH5 showed that it has a high structural homology with hZα$_{ADAR1}$ (Figure 4A). However, GH5 formed insoluble aggregates when mixed with DNA, making it impossible to perform an *in vitro* B–Z transition assay. In a previous study of linker histones, mutations of positively charged residues to uncharged ones were shown to overcome this aggregation problem (50). Similarly, we mutated five residues of GH5 (K41G, S42G, R43G, K53A and R95A) to improve the solubility of the GH5/DNA complex (referred to as GH5* hereinafter). As these mutated residues are not located on the Z-DNA binding interface when the GH5 structure was aligned to the Zα domain structure, we reasonably assumed that they would not be involved in Z-DNA binding after engineering. We successfully purified GH5* and performed B–Z transition assays. In the CD spectrum, the DNA duplex containing CG repeats showed a B-conformation of DNA in the presence of GH5*, indicating that GH5* does not have B–Z transition ability (Figure 4B).

To engineer GH5* to be a Z-DNA binder, we first designed a chimeric mutant GH5*N:hZα$_{ADAR1}$C that consists of the N-terminal half (α1–β1–α2) of GH5* and the C-terminal half (α3–β2–β3) of hZα$_{ADAR1}$ (Supplementary Figure S10). This mutant showed a comparable B–Z transition activity to hZα$_{ADAR1}$ (Figure 4B). Thus, we concluded that this chimeric protein is well-folded and presumably has a similar wHTH motif structure to hZα$_{ADAR1}$. Two series of GH5* mutants were constructed to have Z-DNA binding and B-to-Z conversion ability. The first mutant (denoted as GH5*:α3N$_{ADAR1}$) was designed to have the N-terminal part of the α3 helix (K169–S178) of hZα$_{ADAR1}$ substituted for the corresponding region of GH5*. The second mutant was designed to have the key Z-DNA-contacting residues of hZα$_{ADAR1}$ (K169, K170, N173, R174 and Y177) in the α3 helix of GH5* (denoted as GH5*-KKNRY). Subsequently, additional substitutions in the β-wing region were introduced into each mutant. These were denoted as -PPW, -PW and -W, indicating that they contain P192/P193/W195, P192/W195 and W195 of hZα$_{ADAR1}$, respectively (Supplementary Table S1 and Supplementary Figure S10).

B–Z transition activities of these two series of mutants are summarized in Table 3 (Figure 4C and D). The results confirmed the importance of Z-DNA-contacting amino acids located in the β-wing. Among PPW residues in the β-wing, the tryptophan appears to be essential for B–Z transition as expected, since it is the crucial residue for both protein stability and DNA binding by direct interaction with the key tyrosine residue and water-mediated interaction with the phosphate backbone (18,25,31–38). In GH5*, phenylalanine (F94) replaces the tryptophan (W195 in hZα$_{ADAR1}$). Consistently, the W195F mutation of hZα$_{ADAR1}$ was shown to reduce B–Z transition activity significantly (unpublished data), suggesting that phenylalanine cannot fully replace the tryptophan residue in this position.

In our effort to create a GH5* mutant that enables B–Z transition with minimal substitutions, two mutants are noteworthy. One is GH5*-KKNRY-PPW, which has 8 substituted amino acids (K169, K170, N173, R174, Y177, P192, P193 and W195 of hZα$_{ADAR1}$) that are essential for Z-DNA contacts based on the structure of the Zα/Z-DNA complex (18,25,31–38). This mutant has a good B–Z transition activity (Figure 4D and Table 3). The other mutant, GH5*-KKNRY-W, having K169, K170, N173, R174, Y177 and W195 of hZα$_{ADAR1}$, showed substantial B–Z transition activity despite the absence of two Pro residues (P192 and P193 of hZα$_{ADAR1}$) in the β-wing (Figure 4D and Table 3). Although P192 and P193 (as well as T191) were defined as Z-DNA contacting residues in hZα$_{ADAR1}$, they are deficient in a few Zα family members. Thus, the less conserved Pro residues in the β3 strand do not ap-

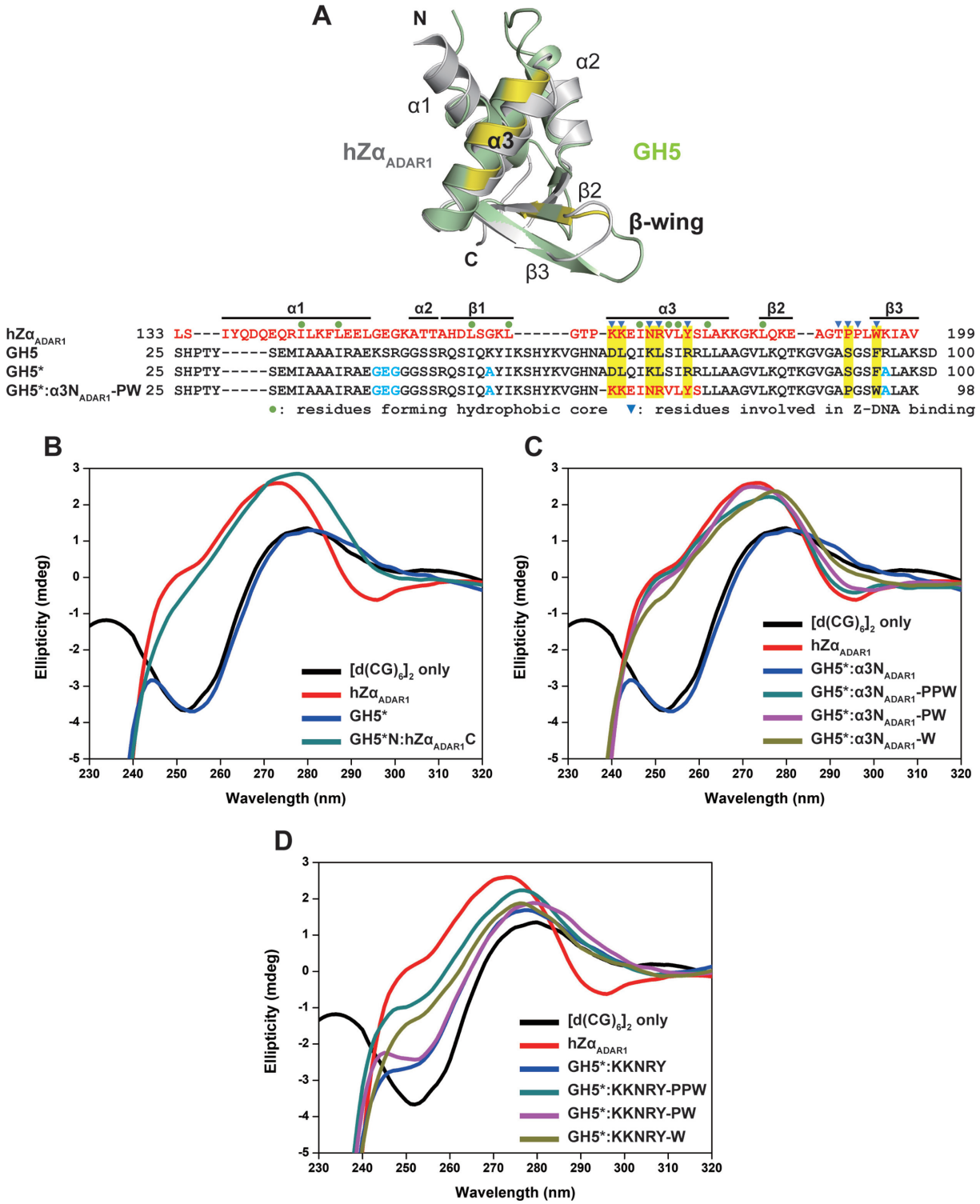

Figure 4. Design of GH5 mutants and their CD spectra. (**A**) Structures of free GH5 (PDB ID 1HST, pale green) and hZα$_{ADAR1}$ (PDB ID 1QBJ, gray) were aligned. Although these two proteins share about 12% sequence identity and have different loop lengths, the overall structures were well aligned, with an RMSD of 1.9 Å. Sequence alignment of hZα$_{ADAR1}$, GH5, GH5*, and GH5*:α3N$_{ADAR1}$-PW is shown below. In the chimeric mutant, residues derived from hZα$_{ADAR1}$ are in red. Mutated residues in GH5* are in cyan. Residues involved in interaction with Z-DNA in hZα$_{ADAR1}$/Z-DNA complex, but not conserved in GH5 and GH5* are highlighted in yellow. CD spectra of the DNA duplex measured in the presence of (**B**) GH5* and GH5*N:hZα$_{ADAR1}$C, (**C**) GH5*:α3N$_{ADAR1}$-series mutants and (**D**) GH5*:KKNRY-series mutants are presented. GH5* has no B–Z transition activity, while its mutants that contain crucial residues for the Z-DNA interaction in the α3 helix and the β-wing show clear B–Z transition activities. The sequences of GH5*N:hZα$_{ADAR1}$C, GH5*:α3N$_{ADAR1}$-series mutants, and GH5*:KKNRY-series mutants are provided in Supplementary Table S1 and Supplementary Figure S10.

Table 3. Relative B–Z transition activity of each GH5* mutant compared to that of hZα$_{ADAR1}$

Protein	B–Z conversion (%)
hZα$_{ADAR1}$	100±3.8[a]
GH5*	0±0.1
GH5*N:hZα$_{ADAR1}$C	91±3.4
GH5*:α3N$_{ADAR1}$	0±0.0
GH5*:α3N$_{ADAR1}$-W	87±3.3
GH5*:α3N$_{ADAR1}$-PW	94±3.6
GH5*:α3N$_{ADAR1}$-PPW	97±3.7
GH5*-KKNRY	28±1.1 (37±1.4[b])
GH5*-KKNRY-W	61±2.3
GH5*-KKNRY-PW	31±1.2 (58±2.1[b])
GH5*-KKNRY-PPW	73±2.8

[a]The relative B–Z transition activity compared to that of hZα$_{ADAR1}$ at a [P]/[N] ratio of 4.
[b]The numbers in parentheses indicate the B–Z transition activity at a [P]/[N] ratio of 30.

pear to be essential for the B–Z transition activity. As expected from the importance of highly conserved tryptophan residue, the GH5*-KKNRY lacking W195 in the β3 strand showed much lower B–Z transition activity. Consequently, a Z-DNA binding protein was artificially built with a defined positional display of essential Z-DNA-contacting residues on the backbone of a precisely defined structure that belongs to WHD.

Z-DNA binding affinity of engineered chimeric GH5

In the previous section, we showed that an α3-swapped vvZα$_{E3L}$ mutant with B–Z transition activity acquired B-DNA binding ability. Similarly, we analyzed Z- and B-DNA binding affinities of GH5*:α3N$_{ADAR1}$-PW, which showed an almost identical B–Z transition CD spectrum to that of hZα$_{ADAR1}$ (Figure 4C). To overcome the aggregation problem during MST, the experiments were carried out in relatively high salt conditions (100 mM NaCl) compared to other experimental conditions for vvZα$_{E3L}$ mutants and hZα$_{ADAR1}$ (20 mM NaCl). As a control, the Z-DNA binding affinity of hZα$_{ADAR1}$ was measured at high salt conditions, and it showed a much higher K_D value (K_D of 600 nM) than that measured in the 20 mM NaCl condition (K_D of 18 nM). The B-DNA binding affinity of hZα$_{ADAR1}$ was reduced 13-fold (K_D of 35 μM) at high salt conditions, suggesting that the polar interactions of hZα$_{ADAR1}$ are important for Z- and B-DNA binding. MST experiments with GH5*:α3N$_{ADAR1}$-PW showed that this GH5 chimera acquired a Z-DNA binding ability with a K_D of 1.8 μM, which is just three times lower than that for hZα$_{ADAR1}$ (Table 4 and Supplementary Figure S11). The B-DNA binding affinity of GH5*:α3N$_{ADAR1}$-PW is similar to that of hZα$_{ADAR1}$ with K_D of 31 μM (Table 4 and Supplementary Figure S11). On the other hand, we also compared the binding affinities of GH5* and GH5*:α3N$_{ADAR1}$-PW with B-DNA using MST to confirm whether or not a change in B-DNA binding ability occurred by engineering of the GH5* chimera from GH5*. An initial trial to measure the B-DNA binding affinity of GH5* under 100 mM NaCl conditions failed due to aggregation during MST. Thus, we performed MST experiments in 150 mM KCl conditions, where the binding

Table 4. DNA binding affinity of hZα$_{ADAR1}$ and GH5* mutant

Protein	Z-DNA binding affinity (μM)	B-DNA binding affinity (μM)
hZα$_{ADAR1}$	0.60 ± 0.07	35 ± 3
GH5*:α3N$_{ADAR1}$-PW	1.8 ± 0.2	31 ± 2

Experiments were performed at 22°C with a buffer consisting of 20 mM HEPES (pH 8.0), 100 mM NaCl, 0.5 mg/ml BSA, and 0.05% Tween20.

Table 5. B-DNA binding affinity of GH5* and GH5* mutant

Protein	B-DNA binding affinity (μM)
GH5*	167 ± 50
GH5*:α3N$_{ADAR1}$-PW	144 ± 16

Experiments were performed at 22°C with a buffer consisting of 20 mM Tris-Cl (pH 7.8), 150 mM KCl, 0.5 mg/ml BSA, and 0.05% Tween20.

affinity between the globular domain of H1 and linear 30 bp DNA was measured previously (51). In this condition, we confirmed that GH5* and GH5*:α3N$_{ADAR1}$-PW have similar binding affinities to B-DNA (Table 5 and Supplementary Figure S12).

Altogether, by mutating the 12 amino acids of GH5*, we successfully engineered GH5*, the B-DNA binder, into a hZα$_{ADAR1}$-like protein with a Z-DNA binding affinity similar to that of hZα$_{ADAR1}$ while maintaining the B-DNA binding ability of GH5*.

Crystal structure of engineered GH5 in complex with [*d*(TCGCGCG)]$_2$

To obtain detailed structural information of the interaction between engineered GH5* chimera and Z-DNA, we determined the crystal structure of one of the B-to-Z converting mutants, GH5*:α3N$_{ADAR1}$-PW, in complex with [*d*(TCGCGCG)]$_2$ at a resolution of 2.75 Å (Figure 5A and Supplementary Table S3). Two protein molecules and one duplex DNA molecule, [*d*(TCGCGCG)]$_2$, are present in an asymmetric unit of the crystal lattice. In this complex, DNA was shown to form typical Z-conformation with alternating *anti*- and *syn*-conformations of nucleotides and was structurally well aligned to the hZα$_{ADAR1}$-bound Z-DNA (Supplementary Table S4), demonstrating that this GH5* chimera successfully achieved Z-conformation-specific DNA binding in the same manner as hZα$_{ADAR1}$. However, the structural analysis of Z-DNA in complex with GH5* chimera using the web 3DNA 2.0 program (49), showed that the 'Rise' value of each step was constant, unlike the zigzag-shaped graph of the 'Rise' values found in other Z-DNA structures (Supplementary Figure S13). This difference may be caused by the slight movement of the C-terminal half of α3 helix and β-wing, which affects the conformation of their interacting phosphate backbones (Supplementary Figure S14).

This GH5* chimera has a conserved Z-DNA binding interface using the engineered α3 helix (Figure 5B). The well-conserved interactions are mediated by N1173, R1174, and Y1177 of the α3 helix of this chimera, which are derived from hZα$_{ADAR1}$ (Supplementary Figure S15). Similar to the numbering system used in the vvZα$_{E3L}$ chimera, the

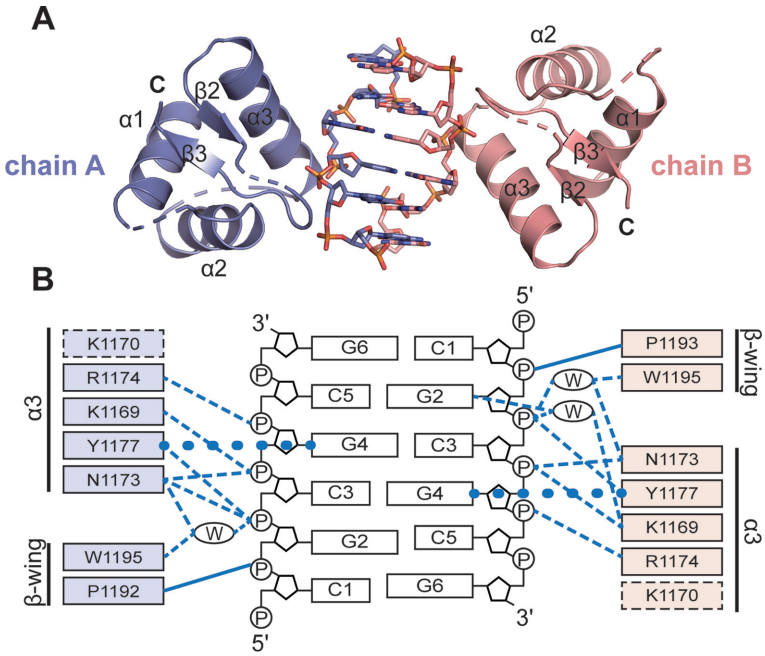

Figure 5. Crystal structure of GH5 mutant in complex with Z-DNA (GH5*:α3N$_{ADAR1}$-PW/Z-DNA). (**A**) The overall structure of GH5*:α3N$_{ADAR1}$-PW complexed with [*d*(TCGCGCG)]$_2$ is shown. Chain A and its binding partner DNA are slate colored, chain B and its binding partner DNA are salmon colored. (**B**) Schematic representation of interactions between protein and DNA. Hydrogen bonds are shown as dashed lines, van der Waals contacts are shown as solid lines, and the CH-π interactions are shown as circled lines. Water molecule within the protein–DNA interface is marked with a W inside the oval. Amino acids derived from hZα$_{ADAR1}$ are indicated by adding 1,000 to the amino acid numbers of hZα$_{ADAR1}$ to clarify that those residues are from foreign protein. Residues involved in Z-DNA binding are indicated by colored boxes and the residue, which does not participate in the interaction with Z-DNA is shown by dotted box.

residues derived from hZα$_{ADAR1}$ in the GH5* chimera are numbered by adding 1,000 to their original residue numbers. On the other hand, interactions of T191 and P193 on the β-wing of hZα$_{ADAR1}$ are missing in this GH5* chimera structure, while the P1192-mediated β-wing interaction is maintained (Figure 5B).

Whereas the overall structural alignment between GH5*:α3N$_{ADAR1}$-PW and hZα$_{ADAR1}$ gives an RMSD of 2.1 Å, the RMSD value for the alignment of the Z-DNA binding interface including the α3 helix and the β-wing is only 0.80 Å. In contrast, the overall alignment of GH5*:α3N$_{ADAR1}$-PW with free GH5 gives a smaller RMSD value than the local alignment involving only the α3 helix and the β-wing (1.2 Å versus 3.3 Å). This large structural deviation in local alignment is caused by a 19.5° rotation of an α3 helix toward Z-DNA in the GH5*:α3N$_{ADAR1}$–PW/Z–DNA complex structure (Supplementary Figure S16). Introduction of Pro in the S91 position (labeled as P1192 in GH5* chimera) induced the formation of a β-wing structure that facilitates the interaction with P2 of Z-DNA. The charge reversal mutation from D66 to K1169 on an α3 helix may promote the movement of the α3 helix toward the Z-DNA backbone by removing the charge repulsion between Asp and the phosphate backbone and introducing an attractive charge interaction between Lys and P4 (Figure 5B). Mutations from R74 to Y1177 and K70 to N1173 induced specific interactions with the G4 base and P4 of Z-DNA, respectively. Other critical mutations to improve Z-DNA binding include L71 to R1174 and F94 to W1195 mutations, the former interacting with P5, and the latter being important for orienting the Tyr side chain to interact with a G4 base.

Our complex structure of a GH5* chimera demonstrated successful engineering of GH5, a B-DNA binder, into a Z-DNA binder by introducing a few Z-DNA contacting residues on the α3N and in a β-wing, while maintaining the overall structural integrity of the wHTH motif of GH5.

DISCUSSION

The Zα domain is known to specifically recognize left-handed nucleic acid duplexes including DNA, DNA/RNA hybrid and RNA. Although biochemical and structural studies on Zα domains clearly demonstrate the Z-conformation specific interactions of Zα domains, the molecular mechanism of B–Z transition by the Zα domain is not fully understood. vvZα$_{E3L}$, the Zα domain of vaccinia viral protein, has an interesting feature in that it binds to Z-DNA using its conserved Z-DNA-interacting residues, but it does not show any B–Z transition activity in physiological conditions even at high excess molar ratios of [P]/[N] (Supplementary Figure S1). In this respect, vvZα$_{E3L}$ is a suitable protein to study B–Z transition activity separately from Z-DNA binding ability. In this study, we successfully transformed vvZα$_{E3L}$ into a functional B-to-Z converter protein by introducing a few point mutations.

This mutational study of vvZα$_{E3L}$ provides two plausible explanations for why vvZα$_{E3L}$ does not have B–Z transition activity. First, vvZα$_{E3L}$ has a relatively loose hydrophobic core, which may cause the key tyrosine residue of the α3

helix to form different rotamers. The vvZα$_{E3L}$-V43I/A46V mutant that could form a more compact hydrophobic core supports this idea because this mutant showed some B–Z transition activity. Apparently, the crystal structure of the vvZα$_{E3L}$ chimeric mutant bound to Z-DNA showed that the key tyrosine residue takes a specific conformation, appropriate for Z-DNA binding, whereas this tyrosine residue showed multiple rotamer conformations in the NMR structure of DNA-free vvZα$_{E3L}$ (Supplementary Figure S17). Second, more importantly, it is conceivable that B-DNA binding may play a significant role in the B–Z transition. We observed that the introduction of positive charges and/or neutralization of a negative charge in the α3C (such as vvZα$_{E3L}$:α3C$_{ADAR1}$ chimera) led to an increased binding affinity for B-DNA. This mutant showed good B–Z transition activity, suggesting that B-DNA binding ability of Z-DNA binding protein is closely correlated with the B–Z transition activity. However, since the vvZα$_{E3L}$:α3C$_{ADAR1}$ mutant also showed enhanced Z-DNA binding affinity, the contribution of Z-DNA stabilization of this mutant to B–Z transition cannot be excluded.

Based on the correlation between B-DNA binding affinity and B–Z transition activity, we postulated that a B-DNA binder could be transformed to be a Zα-like protein if it acquires the Z-DNA binding ability. Using GH5, a B-DNA binder, we created a Zα-like GH5 mutant having both Z-DNA binding and B–Z transition activities by substituting several amino acids located in the α3 helix and β-wing without altering the overall structure of the protein. The engineering of GH5 to a structurally similar but functionally different Zα-like protein was a very intriguing task, especially in terms of changing its ligand conformation specificity. Based on our GH5 engineering results, it appears that structural arrangement of the crucial Z-DNA-contacting residues may be sufficient to have dual-specificity toward the DNA conformation, without the need for modifying the overall structure frame. The crystal structure of the GH5*:α3N$_{ADAR1}$-PW in complex with Z-DNA confirmed that DNA binding proteins with wHTH motifs can be remodeled as a protein with different conformational specificities of DNA while maintaining their overall structures. Consequently, the proteins with a fold wHTH motif such as GH5 could offer a structural basis for creating a novel conformation-specific DNA binding protein. In addition, our result provides an interesting perspective on how nature uses the almost identical tertiary structure to recognize two oppositely-handed conformations of dsDNA. In physiological conditions, Z-DNA formation appears to be dynamic and transient, which would be suitable for a regulatory module to instruct momentary and timely controls over biological processes such as gene expression and genetic control of metabolic networks. By extending our study, it would be interesting to create sequence-specific Z-DNA binders that enrich the usefulness of Z-DNA binders as Z-DNA-based gene expression circuits and control devices for therapeutic and synthetic biological tools.

We showed that the Zα domain with a B–Z transition activity has B-DNA binding ability, but the molecular mechanism of B-DNA binding involved in the B–Z transition process is not clear. Since structural information of the B-DNA-bound Zα domain is not available, we could not directly compare Z-DNA binding interface of Zα domain with its B-DNA binding interface. However, using the crystal structures of chromatosome containing B-DNA-bound GH5 (PDB ID 4QLC and 5WCU) (52,53), it is possible to compare the B-DNA binding mode of GH5 with Z-DNA binding mode of the GH5* chimera. Chromatosome structures showed that GH5 had three binding interfaces, one of which involves α3 and the β-wing, similar to the binding interface between Zα protein and Z-DNA (Figure 6A). When this binding interface was compared to that between the GH5* chimera and Z-DNA, three major differences in the DNA binding mode were observed. First, when GH5*:α3N$_{ADAR1}$-PW is aligned to GH5, the most noticeable difference is the β-wing conformation (Figure 6B). Although GH5*:α3N$_{ADAR1}$-PW has a shorter β-wing, it exhibits steric hindrance to the B-DNA phosphate backbone if it binds to B-DNA in the same mode as observed in the structure of the GH5/B-DNA complex. When GH5 is in complex with B-DNA, the bent β-wing facilitates binding of GH5 to both strands of DNA. In contrast, GH5*:α3N$_{ADAR1}$-PW binds to one strand of Z-DNA duplex. Second, when the GH5/B-DNA complex and GH5*:α3N$_{ADAR1}$–PW/Z-DNA complex are aligned with respect to the protein, the DNA strands bound to the α3 helix are in different directions (Figure 6C). Finally, the GH5 residues corresponding to the major Z-DNA binding residues of GH5*:α3N$_{ADAR1}$-PW are hydrophobic or negatively charged residues except for K70 and R74, which correspond to N1173 and Y1177 of GH5*:α3N$_{ADAR1}$-PW, respectively (Figure 6D). This sequence difference prevents GH5 from interacting with the phosphate backbone of Z-conformation. Multiple B-DNA binding interfaces such as those found in the GH5/B-DNA complexes may promote the large structural transition of the DNA backbones, for example, by bending DNA or recruiting multiple Zα proteins. Indeed, the CD data showed that the B–Z transition increases with increasing [P]/[N] ratios before reaching saturation, suggesting the possibility for multiple Zα proteins to bind to B-DNA.

As the first step in the B–Z transition, the Zα proteins bind to B-DNA through the positive or polar residues, followed by a large structural transition of the DNA phosphate backbones. Although it is highly speculative at present, the initial B-DNA interaction with Zα protein may promote partial melting of DNA duplex through base-pair openings. Base pair rotation then occurs to adopt Z-conformation. Previously, it was proposed that base-pair opening is a crucial step for the B–Z transition process (4) and our previous data also implied that the Zα-induced B–Z transition is dependent on base-pair opening (54). Thus, during the B–Z transition process, many conformational variants of DNA, including a partially unpaired DNA may be produced. In this regard, the CD profiles of DNA obtained using the Zα mutants in this study suggest an interesting aspect of the Zα-induced B–Z transition. The CD spectra of DNA in the presence of weak B–Z converters such as vvZα$_{E3L}$:α3N$_{ADAR1}$ differ noticeably from the canonical CD spectrum of Z-DNA (Supplementary Figure S1). In general, it is assumed that all DNAs would adopt Z-conformation under saturation condition when induced by the strong B–Z converters such as hZα$_{ADAR1}$. On the

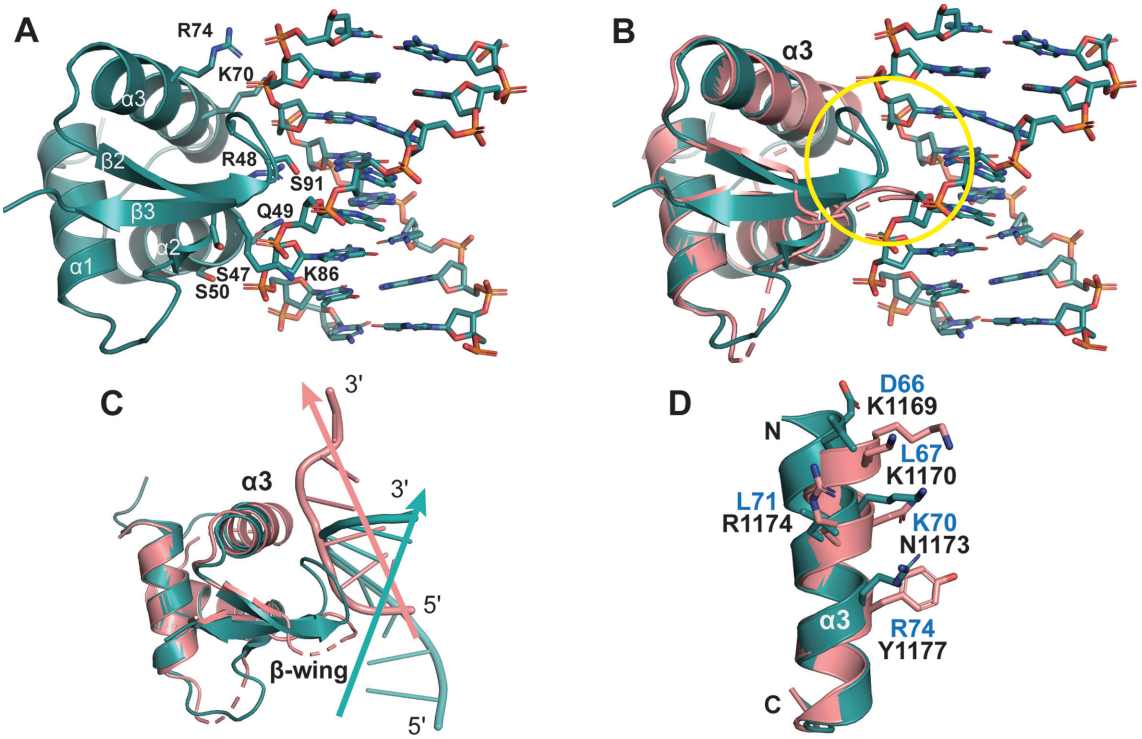

Figure 6. Structural comparison between GH5/B-DNA complex and engineered GH5 mutant/Z-DNA complex. (**A**) The structure of GH5 bound to the phosphate backbone of chromatosome-forming DNA (PDB ID 4QLC (52,53)) is shown. This structure clearly shows the B conformation of DNA. Residues that interact with DNA are represented as sticks (**B**) Structural alignment between GH5*:α3N$_{ADAR1}$-PW (colored in salmon) in complex with Z-DNA and GH5 in complex with B-DNA (colored in teal) reveals steric hindrance between the phosphate backbone of B-DNA and β-wing of GH5*:α3N$_{ADAR1}$-PW, which is marked by a yellow circle. Z-DNA is not shown for clarity. (**C**) Structural alignment between GH5*:α3N$_{ADAR1}$-PW and GH5 indicates different conformations of β-wing and different binding modes for Z-DNA (colored in salmon) and B-DNA (colored in teal). Each arrow represents the central axis of the DNA duplex. The unresolved loop region in the crystal structure is shown as a dashed line. (**D**) Key residues for Z-DNA binding in the α3 helix of GH5*:α3N$_{ADAR1}$-PW (black label) and their corresponding residues of GH5 (blue label) are shown as sticks. It is noteworthy that N1173 and Y1177, which are important for Z-DNA binding in GH5*:α3N$_{ADAR1}$-PW correspond to K70 and R74 of GH5, respectively, which are involved in B-DNA binding.

other hand, the weak B–Z converters, even if excess concentrations are present, do not seem to convert all DNAs to Z-conformation at equilibrium. Thus, the CD spectra of DNA produced by the weak B–Z converters under saturation condition may represent B-DNAs and Z-DNAs as well as partially unpaired DNAs and even single-stranded DNAs stabilized by proteins. At the moment, there is no direct evidence to support our interpretation. Additional studies should be conducted to understand the molecular details of the B–Z transition reaction after B-DNA binding of Zα protein and to interpret this distinguished CD spectral changes.

Overall, our results from the engineering of the two opposite conformation-specific binding proteins, vvZα$_{E3L}$ and GH5, suggest the following conclusion. Paradoxically, Zα-like Z-DNA binding proteins do not rule out B-DNA binding. Rather, engagement with B-DNA may be needed to promote the B–Z transition. How do Zα-like Z-DNA binding proteins then bind to B-DNA? Among diverse DNA binding modes of WHDs, one possibility is that the recognition helix of Zα-like Z-DNA binding proteins could bind at the B-DNA minor groove as observed in the DNA binding domain of human RFX1 transcription factor (55). For now, there are not many clues related to the B-DNA binding mode of Zα-like Z-DNA binding proteins. A study of the complex structure between B-DNA and a Zα-like Z-DNA binding protein may answer this interesting question.

DATA AVAILABILITY

Atomic coordinates and structure factors for the reported crystal structures have been deposited at the Protein Data Bank under accession numbers 7C0I (vvZα$_{E3L}$:α3$_{ADAR1}$/Z-DNA) and 7C0J (GH5*:α3N$_{ADAR1}$-PW/Z-DNA). Other data used in this work are available from the corresponding author upon reasonable request.

SUPPLEMENTARY DATA

Supplementary Data are available at NAR Online.

ACKNOWLEDGEMENTS

We thank the staff at beamline 5C at the Pohang Accelerator Laboratory (PAL) for helping with the X-ray diffraction data collection.

Author contributions: C.P. prepared the protein samples for MST experiments and crystallization, performed MST experiments and crystallization screening, collected and processed diffraction data, and determined the structures.

J.K. assisted in crystallization and diffraction data collection. X.Z. and C.Y.P. carried out construct design, protein expression and purification, and CD measurements of $vvZ\alpha_{E3L}$ mutants (X.Z.) and GH5 mutants (C.Y.P.). S.K.L. and H.W. assisted in protein purification and CD measurements. J.H.C. processed CD data and generated figures. Y.-G.K. and H.-J.C. supervised research, analyzed data and wrote the manuscript with contributions from all authors.

FUNDING

National Research Foundation of Korea (NRF) grants funded by the Korean government (MSIT) [NRF-2015R1A2A2A01008367, NRF-2018R1D1A1B07048910 to Y.-G.K., NRF-2020R1A2C2003783 to H.-J.C.]; Bio & Medical Technology Development Program [NRF-2019M3E5D6063903 to H.-J.C.]. Funding for open access charge: NRF [NRF-2020R1A2C2003783].

Conflict of interest statement. None declared.

REFERENCES

1. Lafer,E.M., Valle,R.P., Moller,A., Nordheim,A., Schur,P.H., Rich,A. and Stollar,B.D. (1983) Z-DNA-specific antibodies in human systemic lupus erythematosus. *J. Clin. Invest.*, **71**, 314–321.
2. Nordheim,A., Pardue,M.L., Lafer,E.M., Moller,A., Stollar,B.D. and Rich,A. (1981) Antibodies to left-handed Z-DNA bind to interband regions of Drosophila polytene chromosomes. *Nature*, **294**, 417–422.
3. Lancillotti,F., Lopez,M.C., Arias,P. and Alonso,C. (1987) Z-DNA in transcriptionally active chromosomes. *Proc. Natl. Acad. Sci. U.S.A.*, **84**, 1560–1564.
4. Wang,A.H., Quigley,G.J., Kolpak,F.J., Crawford,J.L., van Boom,J.H., van der Marel,G. and Rich,A. (1979) Molecular structure of a left-handed double helical DNA fragment at atomic resolution. *Nature*, **282**, 680–686.
5. Haniford,D.B. and Pulleyblank,D.E. (1983) The in-vivo occurrence of Z DNA. *J. Biomol. Struct. Dyn.*, **1**, 593–609.
6. Haniford,D.B. and Pulleyblank,D.E. (1983) Facile transition of poly[d(TG) x d(CA)] into a left-handed helix in physiological conditions. *Nature*, **302**, 632–634.
7. Liu,L.F. and Wang,J.C. (1987) Supercoiling of the DNA template during transcription. *Proc. Natl. Acad. Sci. U.S.A.*, **84**, 7024–7027.
8. Schroth,G.P., Chou,P.J. and Ho,P.S. (1992) Mapping Z-DNA in the human genome. Computer-aided mapping reveals a nonrandom distribution of potential Z-DNA-forming sequences in human genes. *J. Biol. Chem.*, **267**, 11846–11855.
9. Herbert,A., Lowenhaupt,K., Spitzner,J. and Rich,A. (1995) Chicken double-stranded RNA adenosine deaminase has apparent specificity for Z-DNA. *Proc. Natl. Acad. Sci. U.S.A.*, **92**, 7550–7554.
10. Herbert,A., Lowenhaupt,K., Spitzner,J. and Rich,A. (1995) Double-stranded RNA adenosine deaminase binds Z-DNA in vitro. *Nucleic Acids Symp. Ser.*, **33**, 16–19.
11. George,C.X., Ramaswami,G., Li,J.B. and Samuel,C.E. (2016) Editing of cellular self-RNAs by adenosine deaminase ADAR1 suppresses innate immune stress responses. *J. Biol. Chem.*, **291**, 6158–6168.
12. Maruyama,A., Mimura,J., Harada,N. and Itoh,K. (2013) Nrf2 activation is associated with Z-DNA formation in the human HO-1 promoter. *Nucleic. Acids. Res.*, **41**, 5223–5234.
13. Rich,A. and Zhang,S. (2003) Timeline: Z-DNA: the long road to biological function. *Nat. Rev. Genet.*, **4**, 566–572.
14. Ravichandran,S., Subramani,V.K. and Kim,K.K. (2019) Z-DNA in the genome: from structure to disease. *Biophys. Rev.*, **11**, 383–387.
15. Jiao,H., Wachsmuth,L., Kumari,S., Schwarzer,R., Lin,J., Eren,R.O., Fisher,A., Lane,R., Young,G.R., Kassiotis,G. *et al.* (2020) Z-nucleic-acid sensing triggers ZBP1-dependent necroptosis and inflammation. *Nature*, **580**, 391–395.
16. Herbert,A., Alfken,J., Kim,Y.G., Mian,I.S., Nishikura,K. and Rich,A. (1997) A Z-DNA binding domain present in the human editing enzyme, double-stranded RNA adenosine deaminase. *Proc. Natl. Acad. Sci. U.S.A.*, **94**, 8421–8426.
17. Athanasiadis,A. (2012) Zalpha-domains: at the intersection between RNA editing and innate immunity. *Semin. Cell Dev. Biol.*, **23**, 275–280.
18. Schwartz,T., Rould,M.A., Lowenhaupt,K., Herbert,A. and Rich,A. (1999) Crystal structure of the Zalpha domain of the human editing enzyme ADAR1 bound to left-handed Z-DNA. *Science*, **284**, 1841–1845.
19. Schade,M., Turner,C.J., Kuhne,R., Schmieder,P., Lowenhaupt,K., Herbert,A., Rich,A. and Oschkinat,H. (1999) The solution structure of the Zalpha domain of the human RNA editing enzyme ADAR1 reveals a prepositioned binding surface for Z-DNA. *Proc. Natl. Acad. Sci. U.S.A.*, **96**, 12465–12470.
20. Schade,M., Turner,C.J., Lowenhaupt,K., Rich,A. and Herbert,A. (1999) Structure-function analysis of the Z-DNA-binding domain Zalpha of dsRNA adenosine deaminase type I reveals similarity to the (alpha + beta) family of helix-turn-helix proteins. *EMBO J.*, **18**, 470–479.
21. Gajiwala,K.S. and Burley,S.K. (2000) Winged helix proteins. *Curr. Opin. Struct. Biol.*, **10**, 110–116.
22. Berger,I., Winston,W., Manoharan,R., Schwartz,T., Alfken,J., Kim,Y.G., Lowenhaupt,K., Herbert,A. and Rich,A. (1998) Spectroscopic characterization of a DNA-binding domain, Z alpha, from the editing enzyme, dsRNA adenosine deaminase: evidence for left-handed Z-DNA in the Z alpha-DNA complex. *Biochemistry*, **37**, 13313–13321.
23. Kim,Y.G., Lowenhaupt,K., Maas,S., Herbert,A., Schwartz,T. and Rich,A. (2000) The zab domain of the human RNA editing enzyme ADAR1 recognizes Z-DNA when surrounded by B-DNA. *J. Biol. Chem.*, **275**, 26828–26833.
24. Athanasiadis,A., Placido,D., Maas,S., Brown,B.A. 2nd, Lowenhaupt,K. and Rich,A. (2005) The crystal structure of the Zbeta domain of the RNA-editing enzyme ADAR1 reveals distinct conserved surfaces among Z-domains. *J. Mol. Biol.*, **351**, 496–507.
25. Schwartz,T., Behlke,J., Lowenhaupt,K., Heinemann,U. and Rich,A. (2001) Structure of the DLM-1-Z-DNA complex reveals a conserved family of Z-DNA-binding proteins. *Nat. Struct. Biol.*, **8**, 761–765.
26. Quyen,D.V., Ha,S.C., Lowenhaupt,K., Rich,A., Kim,K.K. and Kim,Y.G. (2007) Characterization of DNA-binding activity of Z alpha domains from poxviruses and the importance of the beta-wing regions in converting B-DNA to Z-DNA. *Nucleic. Acids. Res.*, **35**, 7714–7720.
27. Lee,E.H., Seo,Y.J., Ahn,H.C., Kang,Y.M., Kim,H.E., Lee,Y.M., Choi,B.S. and Lee,J.H. (2010) NMR study of hydrogen exchange during the B–Z transition of a DNA duplex induced by the Zalpha domains of yatapoxvirus E3L. *FEBS Lett.*, **584**, 4453–4457.
28. Kim,Y.G., Muralinath,M., Brandt,T., Pearcy,M., Hauns,K., Lowenhaupt,K., Jacobs,B.L. and Rich,A. (2003) A role for Z-DNA binding in vaccinia virus pathogenesis. *Proc. Natl. Acad. Sci. U.S.A.*, **100**, 6974–6979.
29. Kim,Y.G., Lowenhaupt,K., Oh,D.B., Kim,K.K. and Rich,A. (2004) Evidence that vaccinia virulence factor E3L binds to Z-DNA in vivo: Implications for development of a therapy for poxvirus infection. *Proc. Natl. Acad. Sci. U.S.A.*, **101**, 1514–1518.
30. Kahmann,J.D., Wecking,D.A., Putter,V., Lowenhaupt,K., Kim,Y.G., Schmieder,P., Oschkinat,H., Rich,A. and Schade,M. (2004) The solution structure of the N-terminal domain of E3L shows a tyrosine conformation that may explain its reduced affinity to Z-DNA in vitro. *Proc. Natl. Acad. Sci. U.S.A.*, **101**, 2712–2717.
31. Ha,S.C., Lokanath,N.K., Van Quyen,D., Wu,C.A., Lowenhaupt,K., Rich,A., Kim,Y.G. and Kim,K.K. (2004) A poxvirus protein forms a complex with left-handed Z-DNA: crystal structure of a Yatapoxvirus Zalpha bound to DNA. *Proc. Natl. Acad. Sci. U.S.A.*, **101**, 14367–14372.
32. Ha,S.C., Lowenhaupt,K., Rich,A., Kim,Y.G. and Kim,K.K. (2005) Crystal structure of a junction between B-DNA and Z-DNA reveals two extruded bases. *Nature*, **437**, 1183–1186.
33. Ha,S.C., Choi,J., Hwang,H.Y., Rich,A., Kim,Y.G. and Kim,K.K. (2009) The structures of non-CG-repeat Z-DNAs co-crystallized with the Z-DNA-binding domain, hZ alpha(ADAR1). *Nucleic Acids Res.*, **37**, 629–637.
34. de Rosa,M., de Sanctis,D., Rosario,A.L., Archer,M., Rich,A., Athanasiadis,A. and Carrondo,M.A. (2010) Crystal structure of a junction between two Z-DNA helices. *Proc. Natl. Acad. Sci. U.S.A.*, **107**, 9088–9092.

35. de Rosa,M., Zacarias,S. and Athanasiadis,A. (2013) Structural basis for Z-DNA binding and stabilization by the zebrafish Z-DNA dependent protein kinase PKZ. *Nucleic Acids Res.*, **41**, 9924–9933.
36. Kim,D., Hur,J., Park,K., Bae,S., Shin,D., Ha,S.C., Hwang,H.Y., Hohng,S., Lee,J.H., Lee,S. *et al.* (2014) Distinct Z-DNA binding mode of a PKR-like protein kinase containing a Z-DNA binding domain (PKZ). *Nucleic Acids Res.*, **42**, 5937–5948.
37. Kus,K., Rakus,K., Boutier,M., Tsigkri,T., Gabriel,L., Vanderplasschen,A. and Athanasiadis,A. (2015) The structure of the cyprinid herpesvirus 3 ORF112-zalpha.Z-DNA complex reveals a mechanism of nucleic acids recognition conserved with E3L, a poxvirus inhibitor of interferon response. *J. Biol. Chem.*, **290**, 30713–30725.
38. Kim,D., Hur,J., Han,J.H., Ha,S.C., Shin,D., Lee,S., Park,S., Sugiyama,H. and Kim,K.K. (2018) Sequence preference and structural heterogeneity of BZ junctions. *Nucleic. Acids. Res.*, **46**, 10504–10513.
39. Bae,S., Kim,D., Kim,K.K., Kim,Y.G. and Hohng,S. (2011) Intrinsic Z-DNA is stabilized by the conformational selection mechanism of Z-DNA-binding proteins. *J. Am. Chem. Soc.*, **133**, 668–671.
40. Kang,Y.M., Bang,J., Lee,E.H., Ahn,H.C., Seo,Y.J., Kim,K.K., Kim,Y.G., Choi,B.S. and Lee,J.H. (2009) NMR spectroscopic elucidation of the B–Z transition of a DNA double helix induced by the Z alpha domain of human ADAR1. *J. Am. Chem. Soc.*, **131**, 11485–11491.
41. Kim,S.H., Lim,S.H., Lee,A.R., Kwon,D.H., Song,H.K., Lee,J.H., Cho,M., Johner,A., Lee,N.K. and Hong,S.C. (2018) Unveiling the pathway to Z-DNA in the protein-induced B–Z transition. *Nucleic. Acids. Res.*, **46**, 4129–4137.
42. Otwinowski,Z. and Minor,W. (1997) Processing of X-ray diffraction data collected in oscillation mode. *Methods Enzymol.*, **276**, 307–326.
43. Potterton,E., Briggs,P., Turkenburg,M. and Dodson,E. (2003) A graphical user interface to the CCP4 program suite. *Acta Crystallogr. D. Biol. Crystallogr.*, **59**, 1131–1137.
44. Liebschner,D., Afonine,P.V., Baker,M.L., Bunkoczi,G., Chen,V.B., Croll,T.I., Hintze,B., Hung,L.W., Jain,S., McCoy,A.J. *et al.* (2019) Macromolecular structure determination using X-rays, neutrons and electrons: recent developments in Phenix. *Acta Crystallogr D Struct Biol*, **75**, 861–877.
45. Emsley,P. and Cowtan,K. (2004) Coot: model-building tools for molecular graphics. *Acta Crystallogr. D. Biol. Crystallogr.*, **60**, 2126–2132.
46. Williams,C.J., Headd,J.J., Moriarty,N.W., Prisant,M.G., Videau,L.L., Deis,L.N., Verma,V., Keedy,D.A., Hintze,B.J., Chen,V.B. *et al.* (2018) MolProbity: more and better reference data for improved all-atom structure validation. *Protein Sci.*, **27**, 293–315.
47. Jerabek-Willemsen,M., Andre,T., Wanner,R., Roth,H.M., Duhr,S., Baaske,P. and Breitsprecher,D. (2014) MicroScale Thermophoresis: Interaction analysis and beyond. *J Mol Struct*, **1077**, 101–113.
48. Moller,A., Nordheim,A., Kozlowski,S.A., Patel,D.J. and Rich,A. (1984) Bromination stabilizes poly(dG-dC) in the Z-DNA form under low-salt conditions. *Biochemistry*, **23**, 54–62.
49. Li,S., Olson,W.K. and Lu,X.J. (2019) Web 3DNA 2.0 for the analysis, visualization, and modeling of 3D nucleic acid structures. *Nucleic Acids Res.*, **47**, W26–W34.
50. Hayes,J.J., Kaplan,R., Ura,K., Pruss,D. and Wolffe,A. (1996) A putative DNA binding surface in the globular domain of a linker histone is not essential for specific binding to the nucleosome. *J. Biol. Chem.*, **271**, 25817–25822.
51. White,A.E., Hieb,A.R. and Luger,K. (2016) A quantitative investigation of linker histone interactions with nucleosomes and chromatin. *Sci. Rep.*, **6**, 19122.
52. Zhou,B.R., Jiang,J., Feng,H., Ghirlando,R., Xiao,T.S. and Bai,Y. (2015) Structural mechanisms of nucleosome recognition by linker histones. *Mol. Cell*, **59**, 628–638.
53. Zhou,B.R., Jiang,J., Ghirlando,R., Norouzi,D., Sathish Yadav,K.N., Feng,H., Wang,R., Zhang,P., Zhurkin,V. and Bai,Y. (2018) Revisit of reconstituted 30-nm nucleosome arrays reveals an ensemble of dynamic structures. *J. Mol. Biol.*, **430**, 3093–3110.
54. Quyen,D.V., Kim,K.K. and Kim,Y.G. (2006) Sequence-dependent kinetic behavior of protein-induced B-to Z-DNA transition. *Bull. Korean Chem. Soc.*, **27**, 1071–1074.
55. Gajiwala,K.S., Chen,H., Cornille,F., Roques,B.P., Reith,W., Mach,B. and Burley,S.K. (2000) Structure of the winged-helix protein hRFX1 reveals a new mode of DNA binding. *Nature*, **403**, 916–921.